

Characterization and Tuning of Ultra High Gradient Permanent Magnet Quadrupoles

S. Becker,^{1,*} M. Bussmann,² S. Raith,¹ M. Fuchs,¹ R. Weingartner,¹ P. Kunz,³
W. Lauth,³ U. Schramm,² M. El Ghazaly,³ F. Grüner,^{1,4} H. Backe,³ and D. Habs¹

¹*Ludwig-Maximilians University of Munich, 85748 Garching, Germany*

²*Forschungszentrum Dresden-Rossendorf FZD, 01314 Dresden, Germany*

³*Institut f. Kernphysik, Univ. Mainz, 55099 Mainz, Germany*

⁴*Max-Planck Institute of Quantum Optics, 85748 Garching, Germany*

The application of quadrupoles with high field gradients and small apertures requires precise control over higher order multipole field components. We present a new scheme for performance control and tuning, which allows the illumination of most of the quadrupole aperture due to the reduction of higher order field components. Hence, the size of the aperture can be minimized to match the beam size to obtain field gradients of 500 T m^{-1} at good imaging quality. The characterization method based on a Hall probe measurement and a Fourier analysis was cross checked using the high quality electron beam at the Mainz Microtron MAMI.

I. INTRODUCTION

High field gradient compact quadrupoles have recently been subject to an increasing amount of attention, in particular as a compact element for beam manipulation in laser based particle acceleration. With a small aperture, permanent magnet quadrupoles (PMQs) can reach high gradients while maintaining high surface magnetization. A number of design approaches have been developed and realized such as pure PMQs [1, 2] according to the Halbach design [3] or modified (hybrid) Halbach quadrupoles utilizing saturated iron to guide the magnetic field [4, 5].

While being of importance in compact accelerator setups, the main interest in PMQs lies in focusing particle beams of high divergence such as laser accelerated ion [6] and electron beams [7, 8, 9]. The control of the field quality as introduced in this work opens the path for using PMQs as focusing elements in Free-Electron-Lasers (FELs) [10] which demand high quality beam transport systems.

	Electromagnetic-Q	PMQ
Aperture	20 mm	6 mm
Length	300 mm	15 mm
Gradient	40 T m^{-1}	500 T m^{-1}
Total Diameter	300 mm	30 mm

TABLE I: Comparison of a typical electro-magnetic QP and the Miniature PMQ as introduced in [1].

Multipole field components higher than the quadrupole field component (QFC) have distorting effects on the electron beam and therefore increase the beam emittance. These higher order multipole field components (HOMFC) have to be minimized.

Assuming a constant ratio of the HOMFC and the pure quadrupole field component at a given radius, small aperture approaches typically suffer from a strong influence of HOMFCs on the beam quality as the beam size to aperture is large compared to commonly used electromagnetic quadrupoles (Table I).

We present a method of tuning PMQs in order to achieve control over higher order field components, which allows the significant reduction of HOMFC while keeping the ratio of beam size to aperture large.

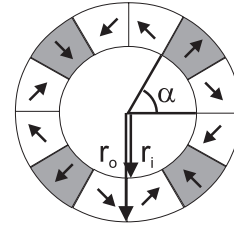


FIG. 1: Design of a miniature quadrupole with 12 permanent magnet wedges. The radius of the aperture is $r_i = 3 \text{ mm}$ and the outer radius is $r_o = 10 \text{ mm}$. The arrows point at the magnetization direction.

Halbach style PMQs were built in-house using 12 wedges (Fig.1) [3]. The permanent magnet material is NdFeB [11] with a remanent field of 1.3 T. The assembled PMQ reaches surface magnetization fields of 1.5 T. The ability to reduce the aperture compared to electromagnetic quadrupoles allows the realization of field gradients of up to 500 T m^{-1} at an aperture of 6 mm diameter. These lenses were preliminarily tested and presented in [1].

Small quadrupole apertures pose challenges in the measurement of the magnetic field distribution. Common approaches include the application of Hall probes to determine the field gradients or rotating coils to determine the HOMFCs. The latter poses challenges in fabrication of the miniature coil and in particular, suppressing vibrations during the measurement [12, 13]. We present a method allowing the measurement of all relevant magnetic vector field components relying solely on a

*Corresponding author; Electronic address: stefan.becker@physik.uni-muenchen.de

miniature Hall probe which can be applied to very small apertures at the required precision. In order to evaluate the accuracy of the measurements, the beam propagation through the measured vector field distribution was simulated using a tracking algorithm [14] and compared to the observed focus of the high quality and well characterized electron beam at the Mainz Microtron MAMI.

The ability to measure all relevant field components within small apertures allows the introduction of specific HOMFCs by changing the position of individual magnet segments. We are thus able to compensate undesired higher field orders and also deliberately introduce specific field components such as octupoles for compensating spherical aberrations or duodecapoles for compensating fringe field effects. Finally, we present experimental results of the quadrupole field tuning. To minimize the influence of the correction of one field component on the entire field distribution, we apply materials with negligible non-linear interactions with the magnetic field due to hysteresis effects.

II. MEASURING FIELD COMPONENTS

The principle presented here for the measurement of the magnetic field involves a Hall probe with an active area of $200\ \mu\text{m}$ in diameter.

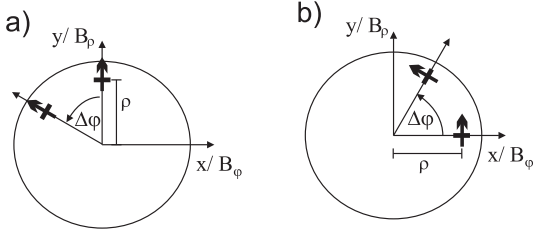


FIG. 2: Measuring scheme of the magnetic vector field in cylindrical coordinates using a Hall probe with the arrow being the surface normal. The radial component (a) as well as the azimuthal component (b) are obtained separately.

The magnetic field is scanned in cylindrical coordinates, as shown in Fig. 2: The original PMQ presented in [1] is mounted on a rotating stage for controlling the φ -coordinate. From the center of rotation, a displacement of the Hall probe along the y-axis scans the radial field component B_ρ , whereas the displacement along the x-axis scans the azimuthal component B_φ . The offset of $\varphi = 90^\circ$ between B_ρ and B_φ has to be considered.

This method requires the precise knowledge of the position of the geometrical center of rotation which not necessarily coincides with the center of the quadrupole magnetic field. In principle, a gradient of $500\ \text{T m}^{-1}$ allows its determination with sub-micrometer precision in spite of the Hall probe having a diameter of $200\ \mu\text{m}$. The tilt error of the probe limits the accuracy to sub $5\ \mu\text{m}$ precision for the simple setup used here. The procedure for finding the geometric center involves a simple

feedback algorithm which only requires the Hall probe signal. The result of this iteration is unique as the field changes monotonously from an arbitrary point inside the aperture.

A. Fourier Analysis

A direct measurement of the entire magnetic field for $0 < \rho < \rho_0$ in cylindrical coordinates inside the aperture overdetermines the magnetic vector field. The assumptions $H = 0$ inside the aperture and $B_z = 0$ lead to the expansion of the magnetic field using polar coordinates of

$$\vec{B}(\rho, \varphi) = \sum_{l=1}^{\infty} [B_{l\rho}(\rho, \varphi) \vec{e}_\rho + B_{l\varphi}(\rho, \varphi) \vec{e}_\varphi] \quad (1)$$

with

$$B_{l\rho}(\rho, \varphi) = \rho^{l-1} [a_l \sin(l\varphi) + b_l \cos(l\varphi)] \quad (2)$$

$$B_{l\varphi}(\rho, \varphi) = \rho^{l-1} [a_l \cos(l\varphi) - b_l \sin(l\varphi)], \quad (3)$$

a_l and b_l being coefficients representing the HOMFCs. The case $B_z \neq 0$ would imply fringe fields, which are discussed in the next section.

Measuring either the B_ρ or the B_φ field component on a single ring (Fig. 3a, b) is sufficient for a complete determination of the magnetic vector field. A Fourier expansion of one ring of radius ρ_0 leads to the desired coefficients a_l and b_l in magnitude $\sqrt{a_l^2 + b_l^2}$ (Fig. 3c) and phase $\arctan(b_l/a_l)$ (Fig. 3d) allowing to construct the vector field (1) using either

$$\begin{aligned} a_l &= \frac{1}{\pi} \int_0^{2\pi} \rho_0^{1-l} B_\varphi(\rho_0, \varphi) \cos(l\varphi) d\varphi \\ b_l &= -\frac{1}{\pi} \int_0^{2\pi} \rho_0^{1-l} B_\rho(\rho_0, \varphi) \sin(l\varphi) d\varphi \end{aligned} \quad (4)$$

or

$$\begin{aligned} a_l &= \frac{1}{\pi} \int_0^{2\pi} \rho_0^{1-l} B_\rho(\rho_0, \varphi) \sin(l\varphi) d\varphi \\ b_l &= \frac{1}{\pi} \int_0^{2\pi} \rho_0^{1-l} B_\varphi(\rho_0, \varphi) \cos(l\varphi) d\varphi. \end{aligned} \quad (5)$$

Those two independent measurements of B_φ and B_ρ must yield the same values for the coefficients a_l and b_l . Differences in these values suggest that the surface normal of the Hall probe is not oriented correctly with respect to the ring being measured (tangential for (4) and perpendicular for (5)).

Knowing the absolute positioning error of the quadrupole center, we obtain a relative error of $\Delta\rho/\rho = 0.5\%$ for $\rho_0 = 1\ \text{mm}$.

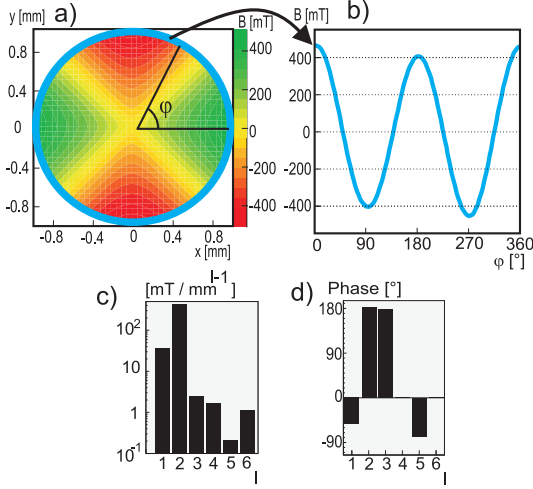


FIG. 3: (a) Field measurements showing the azimuthal component in cylindrical coordinates and (b) its outer-most ring at $\rho = 1$ mm is plotted against one rotation and used to expand the field coefficients a_l and b_l , shown in (c) magnitude $\sqrt{a_l^2 + b_l^2}$ and (d) phase $\arctan(b_l/a_l)$.

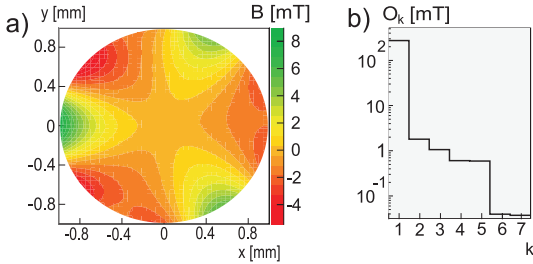


FIG. 4: (a) Azimuthal HOMFC from Fig. 3 ($\vec{B} = \sum_{l=3}^6 [B_{l\rho}(\rho, \varphi)\vec{e}_\rho + B_{l\varphi}(\rho, \varphi)\vec{e}_\varphi]$), note the absolute scale compared to Fig. 3). (b) The remainder after the k^{th} field component.

The measurement errors for B_φ or B_ρ can be estimated by calculating the remainder

$$O_k = \int_0^{2\pi} \left| B_{\rho/\varphi}(\rho_0, \varphi) - \sum_{l=1}^k B_{l\rho/\varphi}(\rho_0, \varphi) \right| d\varphi. \quad (6)$$

For all field measurements performed we find the contribution of orders above the sixth (the duodecapole) to be negligible as shown by the remainder in Fig. 4b. This result is expected from symmetry consideration of the quadrupole design. Hence, the fact that measurement noise or signal drifts would significantly increase the remainder shows that those influences are clearly negligible up to at least the duodecapole order. A simple estimate to determine the maximum order component which can be resolved by a Hall probe with a diameter d_H yields $l_{max} = \pi\rho_0/d_H = 15$ and hence, a resolution well above the duodecapole ($l = 6$).

B. Fringe Fields

The calculation of the field components from the ring measurement (Fig. 3) requires the assumption of $B_z = 0$, see section II A. This means that the ring measurement used for the field expansion must not be performed in the fringe field area of the quadrupole for constructing the field distribution following Eq. 1.

There are cases, however, where fringe fields cannot be neglected, in particular when particle beams are being focused to waist sizes on the nanometer scale. For the Halbach quadrupole, fringe fields are discussed in [3]. In practice, however, this does not determine the effect of fringe fields on a beam in a general way. Even if the quadrupole design is known and hence the ideal fringe fields, the final effect on the beam still depends on the length of the quadrupole and on the beam size and divergence. One solution to this problem is to employ ray-tracing calculations for a specific configuration. An effective higher order field component in the quadrupole can then be determined to fully compensate the effect of the fringe field. This is done by introducing a field component of the same order and magnitude as the fringe field but with a phase shift of 180° .

III. FINAL FOCUS MEASUREMENT AT MAMI ELECTRON BEAM

For confirming the method of expanding magnetic fields from Hall probe measurements, we arranged a PMQ-lens-doublet to focus the electron beam of the electron accelerator MAMI. The beam profile was monitored by a pair of $4 \mu\text{m}$ wires movable longitudinally in the direction of the beam propagation and transversely through the beam, both horizontally and vertically. Bremsstrahlung caused by the beam hitting the wire was detected with an ionization chamber in forward direction. The Bremsstrahlung's intensity, measured while changing the position of the wires transversely to the beam, determines the beam shape at a certain longitudinal position. The MAMI electron beam can reach energies of up to 855 MeV. The beam energy was chosen to be 270 MeV with an energy stability of $\Delta E/E = 10^{-5}$ at an emittance of 2 nmrad horizontally and 0.7 nmrad vertically.

The calculation of the beam transport involves an expansion of the the magnetic fields of the quadrupoles following Eq. 4 and 5 and tracking the electron beam [14], using the the field map given by Eq. 1.

Two beam configurations were chosen: A convergent electron beam of small size at the entrance of the lens-doublet (Fig. 5), and a divergent beam of larger size (Fig. 6).

The measured waist size is only a little larger than that of an ideal quadrupole with the same gradient as expected for the small-beam configuration. The waist size of the transport calculation using the expanded fields

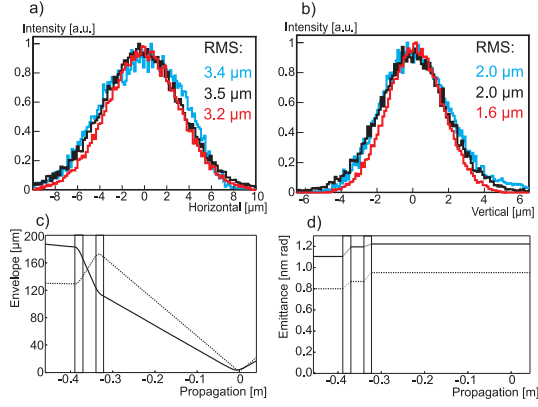


FIG. 5: Small electron beam configuration: (a) Horizontal and (b) vertical beam plane at the waist for the small-beam configuration. Blue: Measured beam. Black: Calculated beam using expanded fields. Red: Calculated beam using ideal fields. (c) The calculated beam envelope and (d) emittance are plotted against the propagation direction of the beam. The vertical lines mark the quadrupole positions.

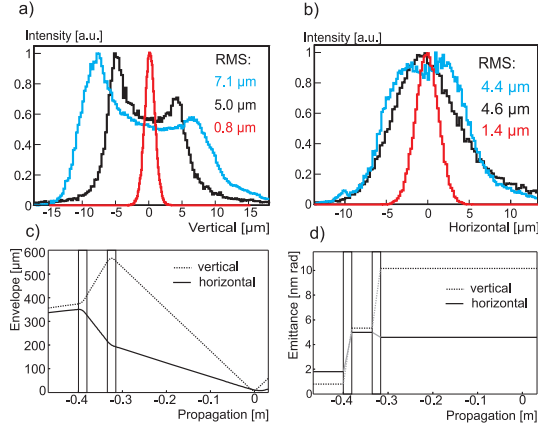


FIG. 6: Large beam configuration: Horizontal (a) and vertical (b) beam plane at the waist for the large-beam configuration. Blue: Measured electron beam. Black: Calculated electron beam using expanded fields. Red: Calculated electron beam using ideal fields. The calculated beam envelope (a) and emittance (b) are plotted against the beam propagation direction, the solid lines being the horizontal and the dashed the vertical beam plane. The vertical lines mark the quadrupole positions.

agrees well with the measured beam waist. The emittance remains virtually constant.

Higher order field components at the large beam configuration significantly distort the electron beam. The ideal waist size is almost an order of magnitude smaller than measured, which can also be seen from the evolution of the emittance calculated (Fig. 6d).

The observed agreement between the measured and calculated beam profiles confirms the field measurement method.

IV. MAGNETIC FIELD TUNING

HOMFCs can have a variety of origins, for example variations of the shape of the wedges or the magnetization direction or strength. The knowledge of the specific origin of an undesired higher order field component is not necessary for its compensation, which is done by introducing a component of the same order and magnitude but with a phase shift of 180° .

Hence, displacing certain wedges introduces well defined higher order field components which can be used for correcting manufacturing deviations of the wedges, the housing or for modeling the magnetic field distribution to correct for spherical aberrations.

A. Wedge Positioning

The four wedges with the magnetic field oriented towards the center of the quadrupole, in the following called positioning wedges, experience centripetal magnetic forces. A thin non-magnetic cylinder is placed in the center of the quadrupole. Its radius defines the radial distance of the wedges from the quadrupole axis (Fig. 7a,b). The positioning wedges are tightened with positioning screws from the quadrupole housing for fixating the cylinder. The center of the magnetic field can be adjusted to coincide with the geometrical center of the quadrupole for the elimination of the dipole field components.

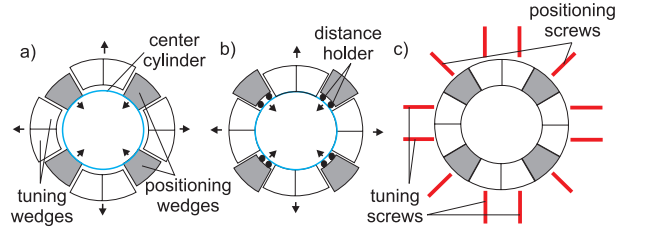


FIG. 7: (a) Arrangement of permanent magnet wedges and the center cylinder (blue). Magnetic forces act centrifugally and centripetally on the wedges. (b) Example for distance holders (e.g. 50-100 μm aluminium foil) of the positioning wedges from the center cylinder. (c) Positioning and tuning screws (red) acting on the wedges.

Magnetic forces centrifugally repel the four remaining pairs of wedges, called tuning wedges in the following. In combination with tuning screws, these forces allow their precise positioning. Since the magnetic forces are acting on the tuning wedges as a pair, the tuning screws are arranged in parallel (Fig. 7c).

B. Introduction of Field Components

Assuming a quadrupole device with undesired field components, one first selects a pair of tuning wedges and

moves them in order to obtain an effect in the field distribution. When moving specific wedges it is beneficial to know the quantitative effect on individual field components including their phase. For this sake, each modified quadrupole is calculated numerically [15] and the result is Fourier-expanded following Eq. 4 and 5. From this a reference table of tuning pair modifications and the corresponding effect on the field distribution is obtained.

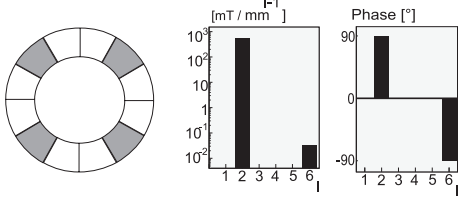


FIG. 8: PMQ is oriented as in Fig. 1. Magnitude and phases of the calculated magnetic field using the ideal arrangement of permanent magnet wedges.

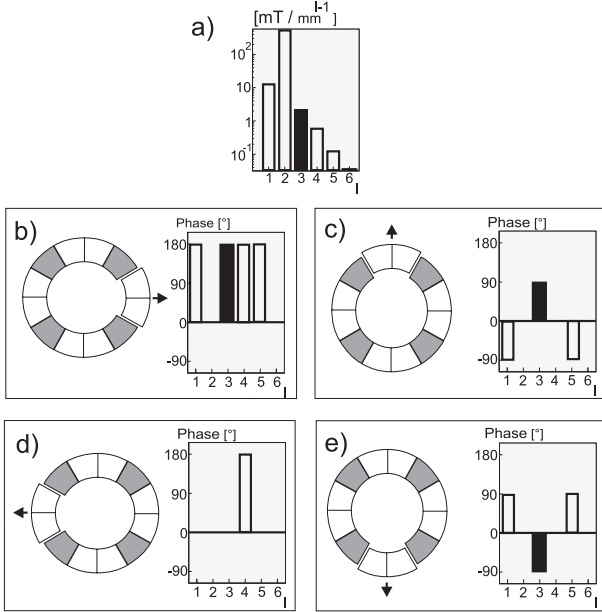


FIG. 9: PMQ is oriented as in Fig. 1. Displacing a single pair of tuning wedges by $150 \mu\text{m}$ introduces a dominant sextupole (l=3). Independent from the specific pairs of tuning wedges displaced, (b) to (e) show the effect on the phases of the introduced field components by moving tuning wedges at $\alpha = 0^\circ, 90^\circ, 180^\circ, 270^\circ$.

Let us first consider the undisturbed quadrupole design in Fig. 8. Owing to the symmetry of the design, only a duodecapole superimposes on the quadrupole field.

Fig. 9 shows that a dominant sextupole ($l=3$) is introduced in case of moving one pair of tuning wedges. For symmetry reasons, we cannot introduce a pure sextupole component. The compensation introduces an octupole field, which can in turn also be eliminated.

The introduction of an octupole component is achieved

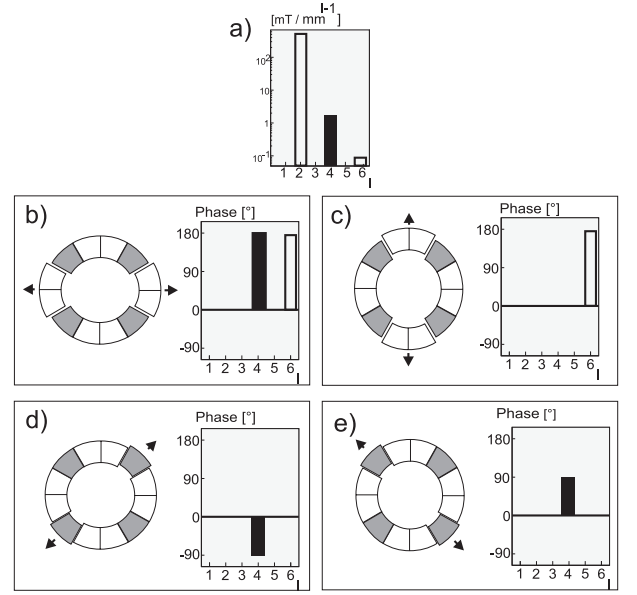


FIG. 10: PMQ is oriented as in Fig. 1. Two opposite pairs of tuning wedges displaced by $150 \mu\text{m}$ introduce a dominant octupole. (a) shows the effect on the magnitude of the field components. (b) and (c) show the effect on the phases of the introduced field components moving tuning wedges at $\alpha = 0^\circ$ and 90° affecting a_4 . Moving the positioning wedges as in d) and e) affect b_4 .

by moving opposite pairs of wedges as shown in Fig. 10. Changing b_4 without influencing a_4 requires the movement of the positioning wedges and thus the need to introduce distance holders, see Fig. 7. Alternatively, b_4 can be modified by moving two individual tuning wedges which are arranged in opposite locations from the device center which requires a subsequent compensation of the additionally introduced a_4 .

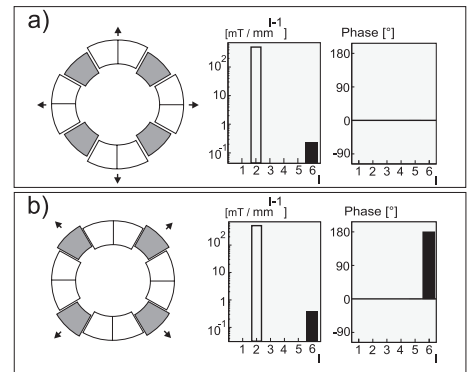


FIG. 11: The PMQ is oriented as in Fig. 1. All pairs of tuning wedges displaced by $150 \mu\text{m}$ introduce a dominant duodecapole. (b) and (c) show distinct pairs of tuning wedges being moved and the effect on magnitudes and phases of the field components. The application of distance holders might be required as in Fig. 7b.

The introduction of a duodecapole field is shown in Fig.

11. Depending on the desired phase, the application of distance holders might be required as shown in Fig. 7b.

C. Adjustment Results

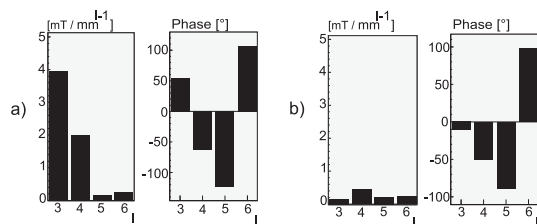


FIG. 12: (a) Higher order magnetic field components within a newly assembled quadrupole. (b) Higher orders are compensated.

Fig. 12a shows an example of a newly assembled quadrupole. Due to manufacturing deviations of either the wedges or the housing, there is a significant initial sextupole component.

After compensating the higher order field components, an almost pure quadrupole field is obtained as shown in Fig. 12, demonstrating the feasibility of the method discussed.

V. CONCLUSION

We have presented a method which allows to shape the magnetic field distribution of a PMQ. A Fourier expansion of the initial magnetic field of the PMQ uniquely

identifies the tuning wedges to be moved for obtaining the desired field distribution. The precise quantification of higher order field components together with the complete control of the field configuration allows to accurately configure the magnetic field distribution to a high degree. After only a few iterations, magnitude and phase of the field components can be reduced significantly.

The quadrupole design and measurement of all relevant field components enables the tuning of PMQs to high precision. Controlling higher order field components up to at least the duodecapole allows a significant larger ratio of the quadrupole's aperture to be illuminated. Moreover, specific higher orders such as an octupole or duodecapole can be introduced in a defined way so that lens aberrations and fringe fields can be compensated for. The advantage of the pure permanent magnet design presented here over hybrid quadrupole designs lies in the linear superposition of the magnetic field contributions of the individual segments. This allows for a decoupled tuning process, and thus for a fast and simple setting of the desired field distribution. The compensation scheme shown here still has potential for improvement since the results presented in this paper were obtained by manually tuning the PMQs. The method for the reduction of HOMFCs can easily be automated using simple algorithms which allow to move the wedges at higher precision.

Acknowledgments

This work has been funded by DFG through transregio TR18 and supported by the DFG cluster-of-excellence Munich Center for Advanced Photonics MAP.

-
- [1] T. Eichner, F. Grüner, S. Becker, M. Fuchs, U. Schramm, R. Weingartner, D. Habs, H. Backe, P. Kunz, W. Lauth, Phys. Rev. ST Accel. Beams **10**, 082401 (2007)
 - [2] J.K. Lim et al, Phys. Rev. ST Accel. Beams **8**, 072401 (2005)
 - [3] K. Halbach, NIM **187** (1981)
 - [4] T. Mihara, Y. Iwashita, M. Kumada, C.M. Spencer Superstrong Adjustable Permanent Magnet for a Linear Collider Final Focus 12th Linear Accelerator Conference. Lubeck, Germany. August 16-20, 2004. SLAC-PUB-10878
 - [5] C.M.S. Sears et al. "Beam Coupling to Optical Scale Accelerating Structures" 12th Advanced Accelerator Concepts Workshop at Lake Geneva, Wisconsin, USA. July 10-15, 2005. SLAC-PUB-12422
 - [6] M. Schollmeier, S. Becker, M. Geissel, K. A. Filippio et al., Phys. Rev. Lett **101**, 055004 (2008)
 - [7] S.P.D. Mangles, C. Murphy, Z. Najmudin, A. Thomas, J. Collier, A. Dangor, E. Divall, P. Foster, J. Gallacher, C. Hooker, D. Jaroszynski, A. Langley, W. Mori, P. Norreys, F. Tsung, R. Viskup, B. Walton, K. Krushelnick, Nature **431**, 535 (2004)
 - [8] C.G.R. Geddes, C. Toth, J. van Tilborg, E. Esarey, C. Schroeder, D. Bruhwiler, C. Nieter, J. Cary, W. Lee-mans, Nature **431**, 538 (2004)
 - [9] J. Faure, Y. Glinec, A. Pukhov, S. Kiselev, S. Gordienko, E. Lefebvre, J.-P. Rousseau, F. Burgy, V. Malka, Nature **431**, 541 (2004)
 - [10] F. Grüner, S. Becker, U. Schramm, T. Eichner, M. Fuchs, R. Weingartner, D. Habs, J. Meyer-ter-Vehn, M. Geissler, M. Ferrario, L. Serafini, B. an der Geer, H. Backe, W. Lauth, S. Reiche, Appl. Phys. B **86**, 431 (2007)
 - [11] Vacuumschmelze Hanau, Vacodym 764 HR data sheets (2005) www.vacuumschmelze.com
 - [12] G. Datzmann et al., NIM B **158** (1999)
 - [13] Y. Iwashita, T. Mihara, M. Kumada, C.M. Spencer "Field Quality and Magnetic Center Stability Achieved in a Variable Permanent Magnet Quadrupole for the Ilc" PAC at Knoxville, TN, USA. May 16-20, 2005. SLAC-PUB-11667
 - [14] General Particle Tracer, www.pulsar.nl
 - [15] CST EM Studio